DOI: 10.13009/EUCASS2022-6054
9TH EUROPEAN CONFERENCE FOR AERONAUTICS AND SPACE SCIENCES (EUCASS)

Reconstruction of the 3D Orientation of a Spinning Sounding Rocket by Detecting the Earth's Horizon and Sun on Onboard Camera Images

Benjamin Braun and Jochen Barf***

German Aerospace Center (DLR), Space Operations and Astronaut Training
Münchener Str. 20, D-82234 Weßling, Germany

** Spaceflight Technology, benjamin.braun@dlr.de*
*** Mobile Rocket Base (MORABA), jochen.barf@dlr.de*

Abstract

The paper describes the reconstruction of the 3D orientation of the spinning PMWE2F sounding rocket solely from the images of a side-looking camera. The Earth nadir vector, pointing to the centre of the Earth, is derived from the detected Earth's horizon hyperbolae, and the Sun direction vector, pointing to the Sun, is derived from the detected Sun ellipses. The orientation is estimated using the TRIAD method when the Earth's horizon and Sun are simultaneously visible, and by determining only two rotational degrees of freedom (DoF) and time interpolation of the third DoF in the meantime when only the Earth's horizon is visible.

1. Introduction

The paper presents a method for reconstructing the three-dimensional orientation of a sounding rocket along its trajectory from the Earth's horizon and the Sun which are detected on the images of an onboard camera, without using gyroscope measurements.

The camera was installed on the one-staged, spinning PMWE2F sounding rocket which was launched from Andøya Space in October 2021. The camera was looking sideways and had been intended to observe the unfolding of the drogue and main chutes at the final descent. Because lift-off took place in the late morning, the Sun was favourably elevated such that it passed just through the centre of the image with every revolution of the spinning rocket during the ascent and coasting phase. Furthermore, since the sounding rocket was in principle upright until the beginning of atmospheric re-entry, the Earth's horizon was continuously visible on the camera images. The sounding rocket was equipped with a GoPro HERO3+ camera.

Hyperbolae and ellipses, respectively, are fitted to the detected Earth's horizon and Sun ellipse curves, from which the direction vectors to the centre of the Earth and to the Sun are derived. By observing these two non-parallel vectors once in an Earth-fixed navigation reference frame and once in a vehicle-fixed frame, the orientation is estimated with the Tri-Axial Attitude Determination (TRIAD) method in the moments when the Earth's horizon and the Sun are simultaneously visible on the camera image. In periods in which only the Earth's horizon is visible, the rotational degree of freedom (DoF) around the direction vector to the centre of the Earth cannot be determined, only the two remaining ones. The rotational DoF about the direction vector to the centre of the Earth that is only discontinuously observable is reconstructed by interpolation over time. To do this easily, a special Earth-fixed coordinate system is introduced, the z -axis of which is aligned with the direction vector to the centre of the Earth. The accuracy is expected to be 2 deg (1σ) about all axes. It is beneficial that the Earth nadir and Sun direction vectors are almost orthogonal.

The development and flight testing of these algorithms is part of MORABA's ongoing efforts to develop a new, more robust and less expensive integrated navigation and attitude/heading reference system for fast spinning sounding rockets. Up until now, MORABA has used an unaided inertial platform as navigation system on the spinning sounding rockets. This platform contains a gimbal on which the gyroscopes and accelerometers are installed and which is rotatable about the roll axis such that the inertial sensors are isolated from the full spin rate. Because the mechanics consisting of bearings, actuators and slip rings is exposed to high loads and vibration during the propelled flight phase, the device is sensitive to damage. The new design uses a strapdown inertial measurement unit (IMU) without any mechanical parts. Since the roll axis gyroscope now experiences the full spin rate, the orientation error of the inertial

DOI: 10.13009/EUCASS2022-6054

navigation solution about the roll axis increases rapidly due to the scaling factor error of the gyroscope. To overcome this deficiency, the inertial navigation system has to be aided by position and velocity measurements of a Global Navigation Satellite System (GNSS) receiver as well as orientation measurements within an integrated navigation system. The 3D orientation estimated from camera images may serve as aiding measurement for such an integrated navigation system.

2. PMWE-2 campaign

The PMWE (Polar Mesospheric Winter Echoes)-2 campaign consisted of two differently instrumented sounding rockets, PMWE2F and PMWE2D, which had already been used in the PMWE-1 campaign as PMWE1F and PMWE1D in April 2018. After a successful recovery in the PMWE-1 campaign, the payloads were overhauled and slightly modified according to the findings of the PMWE-1 campaign for their second use in the PMWE-2 campaign.

The objective of the PMWE-1 and PMWE-2 campaigns was to collect in-situ measurements in the atmospheric layer between 55 and 85 km altitude to better understand the radar echoes which are regularly observed in the North Pole region during the winter season and are most likely caused by neutral air turbulence [1].

During the PMWE-1 campaign, an integrated navigation system consisting of a small, robust strapdown IMU and a GNSS receiver had already been tested on the PMWE1D sounding rocket. The integrated navigation system was aided by Sun direction vector measurements which were derived from the detected Sun ellipses on the camera images of the side-looking camera [2]. On the PMWE1D sounding rocket, soot from the ablative cork coating on the nose cone contaminated the camera lens, resulting in camera images showing only the Sun but not the Earth's horizon. For the PMWE-2 campaign, the nose cones of the PMWE2F and PMWE2D sounding rockets were redesigned so that cork was no longer needed for heat ablation. As a result, there was no more soot on the lens and the Earth's horizon was visible besides the Sun. This enables the estimation of the 3D orientation from the observed Earth nadir and Sun direction vectors, which is presented in this paper. The estimated 3D orientation may be used to aid an integrated navigation system in a similar way as described in [2], which, however, is not the subject of this paper.

The camera images for this analysis were recorded on the PMWE2F sounding rocket that was launched on 1st October 2021 at 10:03:00 (UTC). The flight trajectory is shown in Figure 1. The arrows represent the axes of the body-fixed coordinate system. The rocket was not de-spun after motor burnout but kept up spinning even during the coasting flight phase.

As for the PMWE-1 campaign, the sounding rocket was equipped with a highly accurate inertial navigation platform to provide position, velocity, and orientation. This time, however, the inertial navigation platform failed such that no usable navigation data (and orientation in particular) is available for the experimenters. By processing the camera images, the orientation can be provided to the experimenters at least during the interesting coasting phase, despite the malfunction. However, this orientation estimate is less accurate than that of the inertial navigation platform.

The Earth nadir and Sun direction vector measurements are derived from the captured images of a GoPro HERO3+ camera. Although this camera is not intended for the use on sounding rockets, it provides surprisingly good pictures. This is mainly due to the high resolution and the fast control of the exposure time, which is required because of the quick changeovers between scenes with dark sky and scenes with bright Sun. The video frame rate was 50 Hz, the image resolution was 1920×1080, the horizontal field of view (FOV) was 118.2 deg, and the vertical FOV was 69.5 deg, which corresponds to an equivalent focal length of 17.2 mm. The video was recorded on SD card and could thus only be used in post-processing after recovery of the payload. In Figure 2, the mounting of the side-looking GoPro HERO3+ camera in the rocket structure is shown. The objective lens is protected by a thin pane of glass.

3. Coordinate systems

Figure 3, Figure 4 and Figure 5 show the used coordinate systems. These are the camera coordinate system (c-frame) and the body-fixed coordinate system (b-frame), both of which are fixed to the vehicle, and the Earth-centred Earth-fixed (ECEF) coordinate system (e-frame), the North-East-Down coordinate system (n-frame) and the specially introduced spherical Earth local tangent plane coordinate system (s-frame), all three of which serve as Earth-fixed navigation reference frames. An auxiliary coordinate system (s'-frame) is required for the estimation of the two rotational DoF from the Earth nadir vector in the moments when only the Earth's horizon is visible on the camera images.

DOI: 10.13009/EUCASS2022-6054

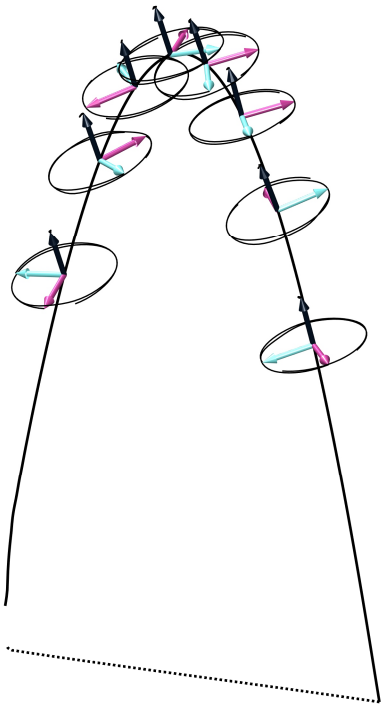

Figure 1: Flight trajectory of the PMWE2F sounding rocket

Figure 2: Side-looking GoPro HERO3+ camera. The lens was protected by a thin pane of glass

The body-fixed coordinate system is located at the reference point of the sounding rocket. The z_b-axis is the roll axis and points to the tip of the rocket. The lateral x_b- and y_b-axes are normal to the longitudinal z_b-axis. At the launch pad, y_b points to the launch rail, and x_b completes the orthogonal right-hand system. The camera coordinate system is located at the focal point of the camera. The z_c-axis is aligned with the line-of-sight of the camera and is parallel to the y_b-axis. The orthogonal x_c- and y_c-axes lie in the image plane of the camera. x_c points to the right and y_c to the bottom of the image.

The current position $\mathbf{x}$ of the sounding rocket and the position of the Sun $\mathbf{X}$ are usually specified in the WGS84 ECEF coordinate system.

The origin O_s of the spherical Earth local tangent plane coordinate system is at the current position $\mathbf{x}$, the z_s-axis points to the centre of the Earth, the y_s-axis points to the East, and the x_s-axis completes the orthogonal right-hand system. Note that this coordinate system slightly differs from the classic local tangent plane coordinate system of the ellipsoidal Earth, the North-East-Down coordinate system.

DOI: 10.13009/EUCASS2022-6054

Given the current position $\mathbf{x}_e = \begin{pmatrix} x_e & y_e & z_e \end{pmatrix}^{\mathrm{T}}$, the longitude λ and the spherical latitude θ are calculated by

$$\lambda = 2\arctan2\left(y_e, x_e\right) = \begin{cases} 2\arctan\dfrac{\sqrt{x_e^2 + y_e^2} - x_e}{y_e} & , \quad y_e \neq 0 \\ 0 & , \quad y_e = 0 \end{cases} \tag{1}$$

$$\theta = \arcsin\frac{z_e}{\left\|\mathbf{x}_e\right\|}$$

A general vector $\mathbf{e}_s$, specified in s-frame, is transformed to e-frame by

$$\mathbf{e}_e = \mathbf{R}_{es}\ \mathbf{e}_s \tag{2}$$

with the transformation matrix

$$\mathbf{R}_{es} = \begin{pmatrix} -\cos\lambda\sin\theta & -\sin\lambda & -\cos\lambda\cos\theta \\ -\sin\lambda\sin\theta & \cos\lambda & -\sin\lambda\cos\theta \\ \cos\theta & 0 & -\sin\theta \end{pmatrix} \tag{3}$$

Rotating the s-frame around the z_s-axis by the rotation angle ψ_{sb} yields the s'-frame. The b-frame is reached by further rotating the s'-frame, first around the $y_{s'}$-axis by the rotation angle ϑ_{sb} and then around the auxiliary x''-axis by the rotation angle φ_{sb}.

The North-East-Down coordinate system is here only used in the end to illustrate the resulting rotation angles in the navigation reference coordinate system that is commonly used for orientation representation.

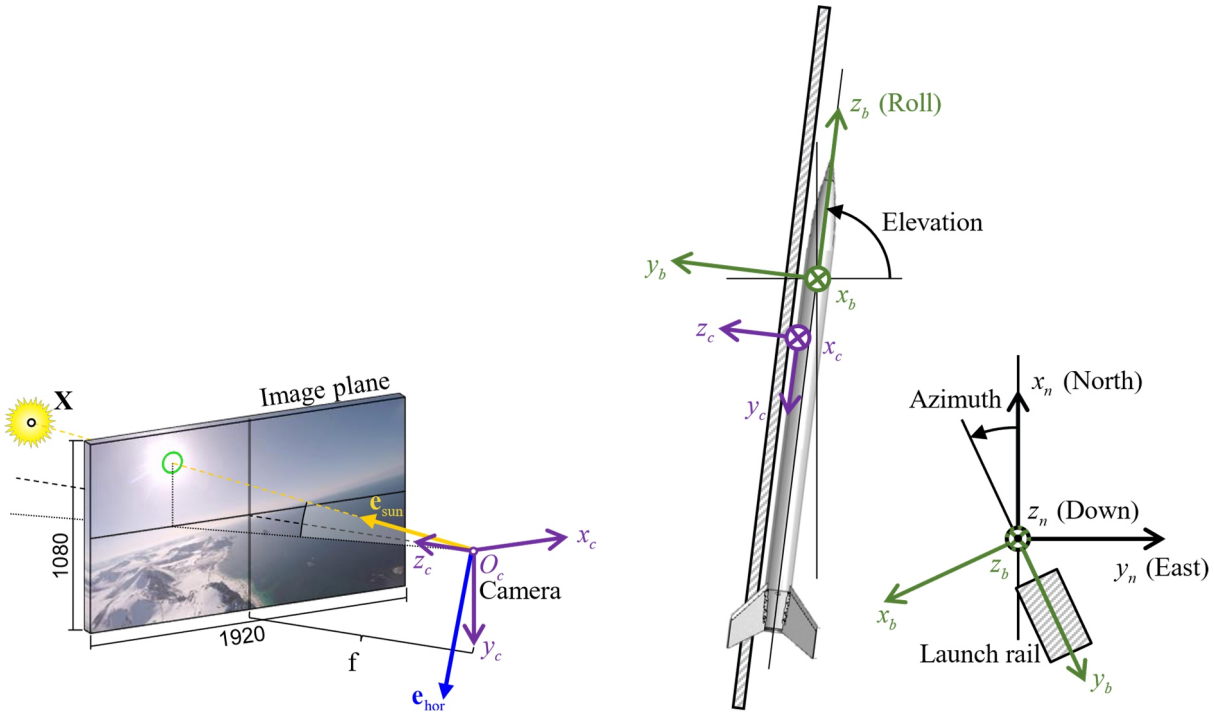

Figure 3: Camera coordinate system (c-frame), body-fixed coordinate system (b-frame) and North-East-Down coordinate system (n-frame)

DOI: 10.13009/EUCASS2022-6054

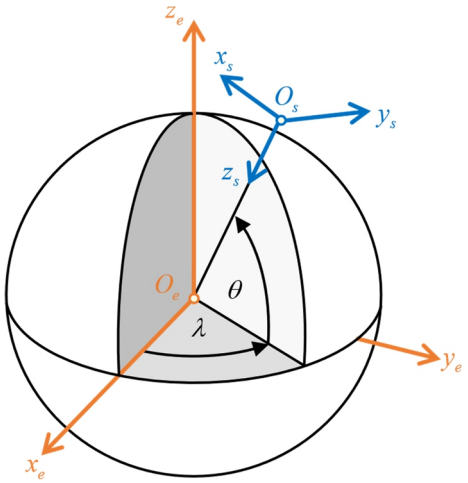

Figure 4:ECEF coordinate system (e -frame) and spherical Earth local tangent plane coordinate system (s -frame). The z_s -axis points to the centre of the Earth

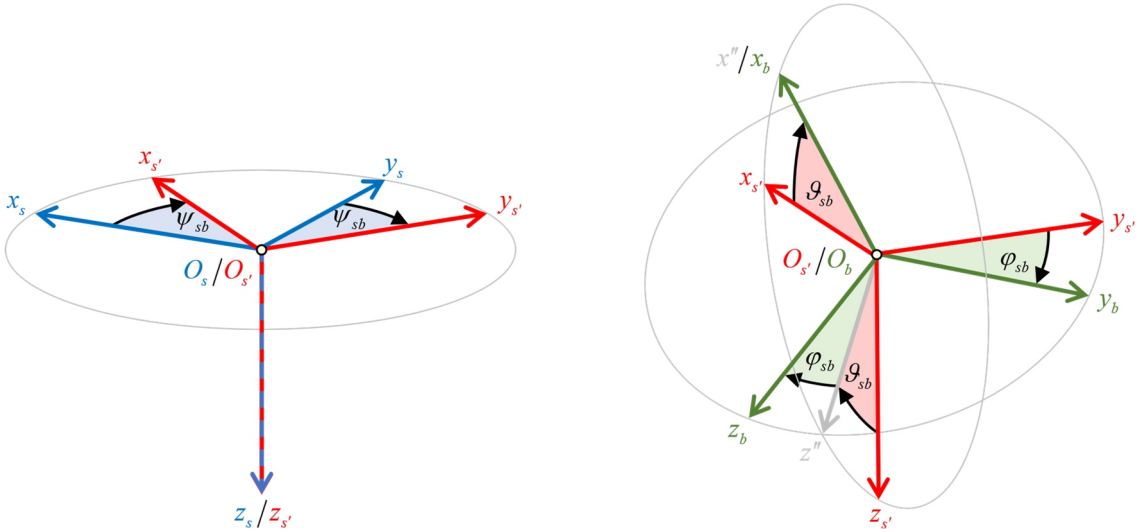

Figure 5: Spherical Earth local tangent plane coordinate system rotated by ψ_{sb} about the z_s -axis (s' -frame)

4. Earth nadir vector

The image processing sequence is exemplarily illustrated in Figure 6. Figure 6a shows the original, distorted image of the Earth's horizon from the camera at T+169s. At first, the image is converted into a binary black-and-white image by applying the given threshold and all contiguous edges between black and white areas are found. Using the fact that the Earth is only partially and not fully visible on the images of sounding rockets due to their low flight height, the algorithm takes only lines into account that intersect the image border. They are shown as blue lines. In a next step, the edges are broken down into individual edges that each meet the condition of beginning and ending at one of the borders of the image. The curves isolated in this way then serve as potential candidates for the Earth's horizon. They are illustrated as coloured curves in Figure 6c. Finally, the curve that best fits a hyperbola is selected as most likely Earth's horizon candidate. The selected curve is undistorted using the intrinsic and extrinsic camera parameters that have been determined before by means of calibration (Figure 6d). Figure 6e shows the undistorted image together with the detected Earth's horizon hyperbola.

From the detected Earth's horizon hyperbola, the Earth nadir vector to the centre of the Earth $\tilde{\mathbf{e}}_{\mathrm{hor},c}$ is derived [3]. Figure 7 shows the three components of the measured Earth nadir vector $\tilde{\mathbf{e}}_{\mathrm{hor},c}$ during the coasting phase between T+50 s and T+280 s. The vector has been normalized to unit length. As expected, the value of the y_c -component is close to +1 during the coasting phase, which means that the sounding rocket is more or less upright and the centre of the Earth is underneath. The oscillations seen in all three components of the Earth nadir vector are due to precession and superimposed nutation motion of the sounding rocket. The Earth's horizon is continuously visible on the camera images, so Earth nadir vector measurements are available at 50 Hz, the frame rate of the video.

DOI: 10.13009/EUCASS2022-6054

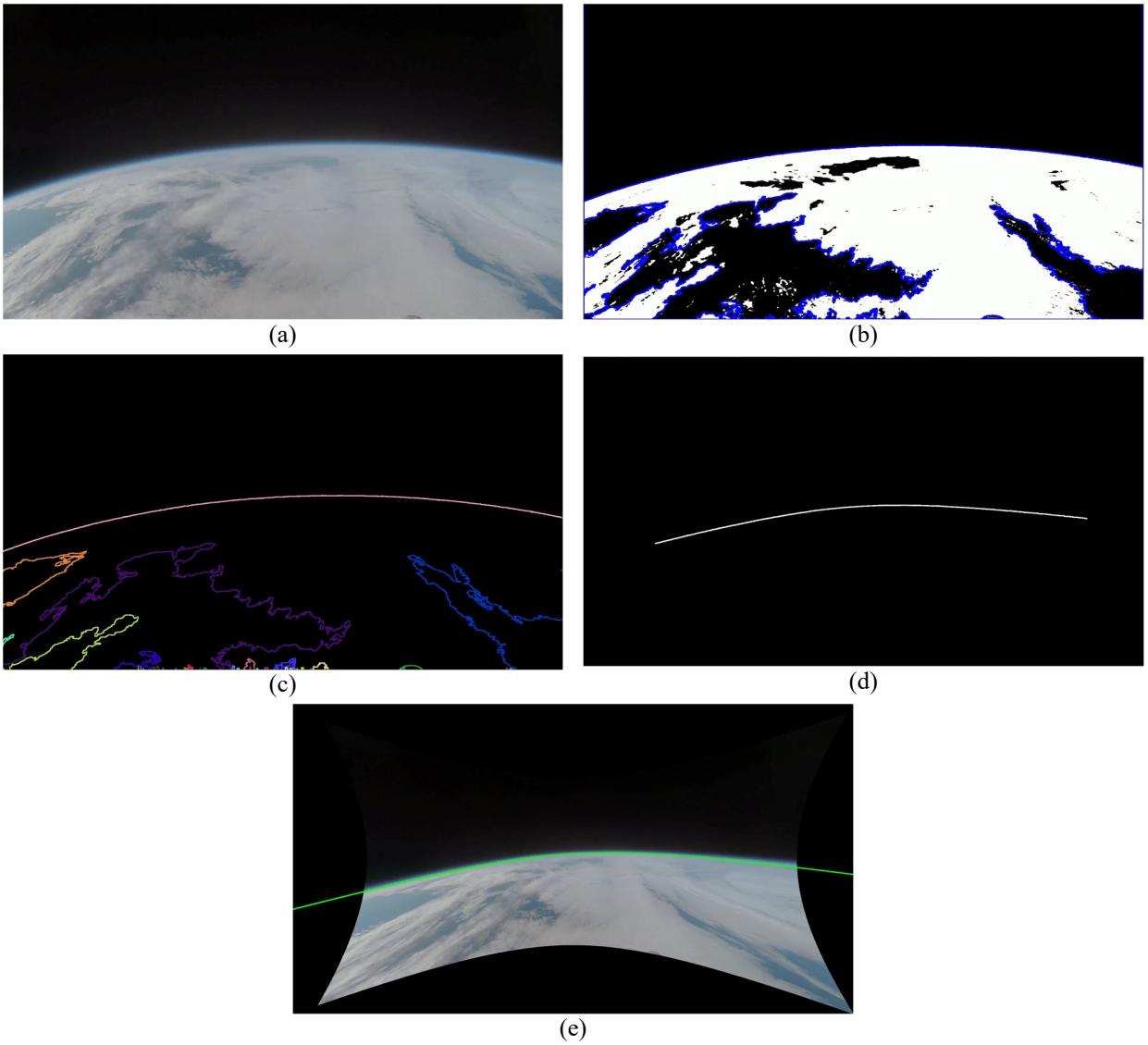

Figure 6: Image processing sequence for detecting the Earth's horizon and determining the Earth nadir vector

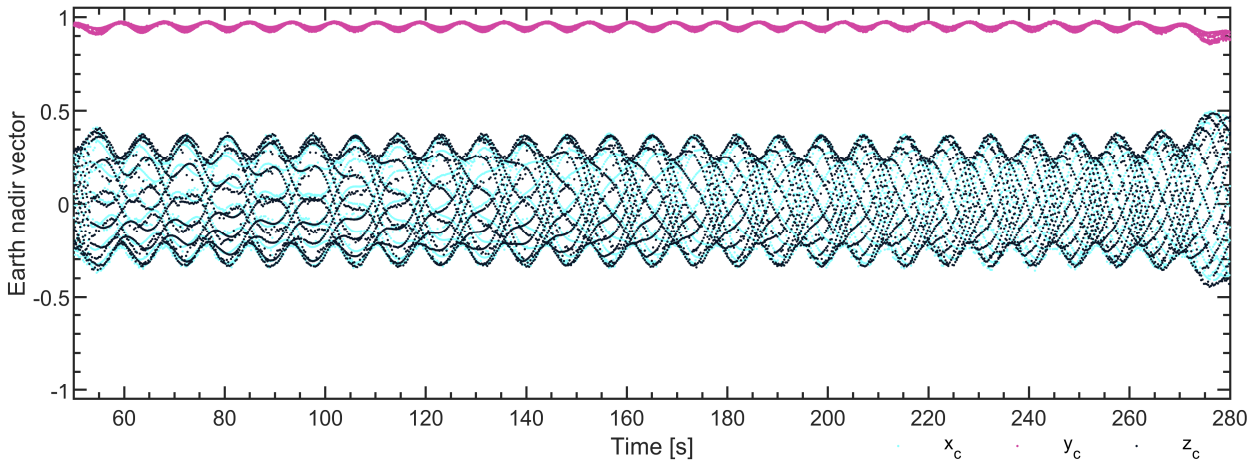

Figure 7: Components of the Earth nadir vector $\tilde{\mathbf{e}}_{\mathrm{hor},c}$ in the coasting phase between T+50 s and T+280 s

DOI: 10.13009/EUCASS2022-6054

5. Sun direction vector

The Earth's horizon detection algorithm has been adapted to also be able to detect the Sun in the camera image. In this case, instead of a hyperbola, the algorithm searches for an ellipse that best fits the found curve. The single processing steps are exemplarily illustrated in Figure 8 for an image taken at T+169 s. The original image from the camera, which is still distorted as can easily be seen form the opposite curvature of the horizon, is shown in Figure 8a. Because the ellipse of the Sun is a closed curve and does not normally intersect the image boundary, as required by the Earth's horizon detection algorithm, the binary image is sectioned into stripes that are less high than the expected projection of the Sun, as shown in Figure 8b. Now, there is a curve that intersects the borders of the stripes and the horizon detection algorithm can be used in the same way as for the Earth's horizon detection. In Figure 8c, the image is undistorted using the intrinsic and extrinsic camera parameters and the closed curved which is most likely the ellipse of the Sun is extracted. Finally, in Figure 8d, an ellipse is fit to the found curve and the coordinates of the piercing point of the line-of-sight to the Sun through the image plane are determined.
Figure 9a shows the image plane of the camera with all Sun centre coordinates that were detected between T+50 s and T+280 s (black) and the points that were flagged as valid by the image processing algorithm and that were used for the 3D orientation estimation (green). About 85% of the Sun centre coordinates were determined correctly. Incorrect measurements are caused, for example, by optical disturbances such as lens flares or incorrectly exposed images, so that, for example, the boundary of the cloud cover is erroneously detected as the Sun curve. Vertically, the Sun passes the image slightly above the centre line. Figure 9b shows a sequence of nine Sun centre coordinates 1…9 over three revolutions of the spinning sounding rocket.

The measured Sun direction vector $\tilde{\mathbf{e}}_{\mathrm{sun},c}$ is calculated from the Sun centre coordinates X_c and Y_c (in pixels) with

$$\tilde{\mathbf{e}}_{\mathrm{sun},c} = \begin{pmatrix} X_c/f \\ Y_c/f \\ 1-\sqrt{X_c^2+Y_c^2}/f \end{pmatrix} \tag{4}$$

where f is the focal length of the camera specified in pixels. The vector is normalized to unit length. Figure 10 shows the three components of the measured Sun direction vector $\tilde{\mathbf{e}}_{\mathrm{sun},c}$ in the coasting phase between T+50 s and T+280 s. The y_c-component takes values between 0 and –0.15 in the coasting phase. Its oscillation is due to the precession and nutation motion of the sounding rocket. Note that during each revolution of the spinning sounding rocket, the Sun direction vector measurements are only available in the phases when the Sun is in FOV of the camera, otherwise not.

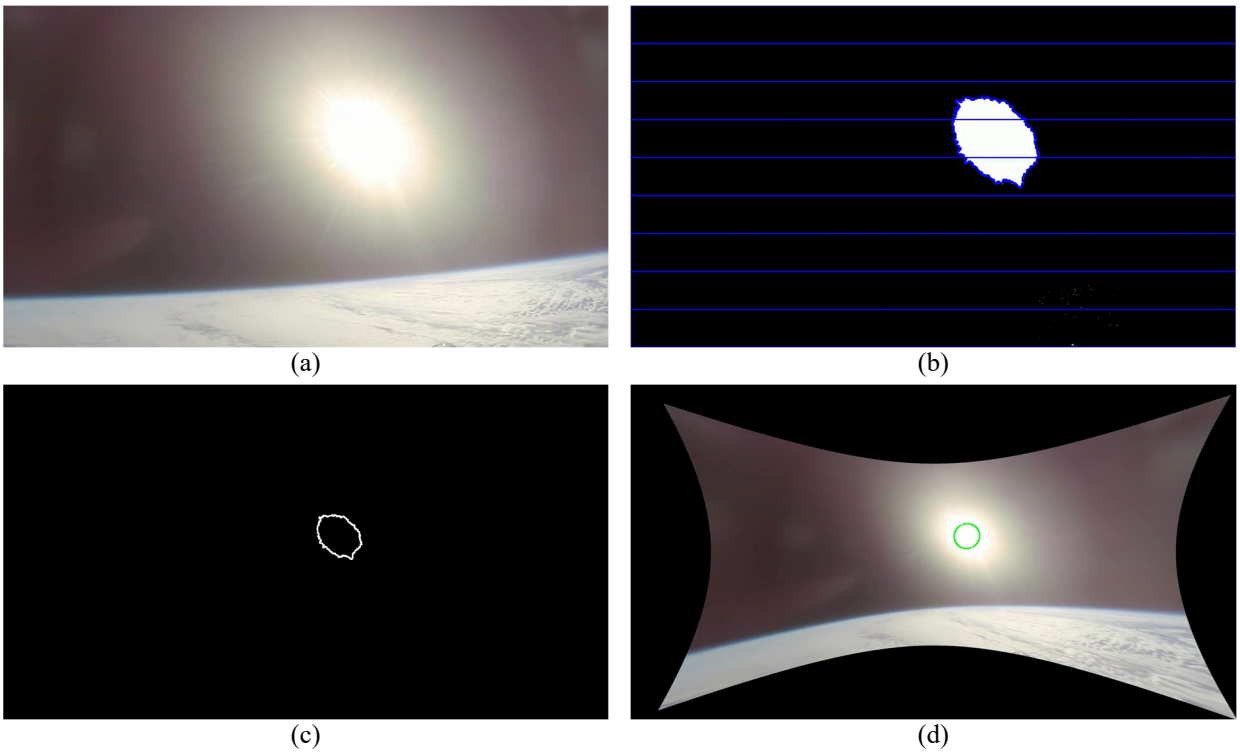

(a) (b) (c) (d)

Figure 8: Image processing sequence for detecting the Sun and determining the Sun direction vector at T+169 s

DOI: 10.13009/EUCASS2022-6054

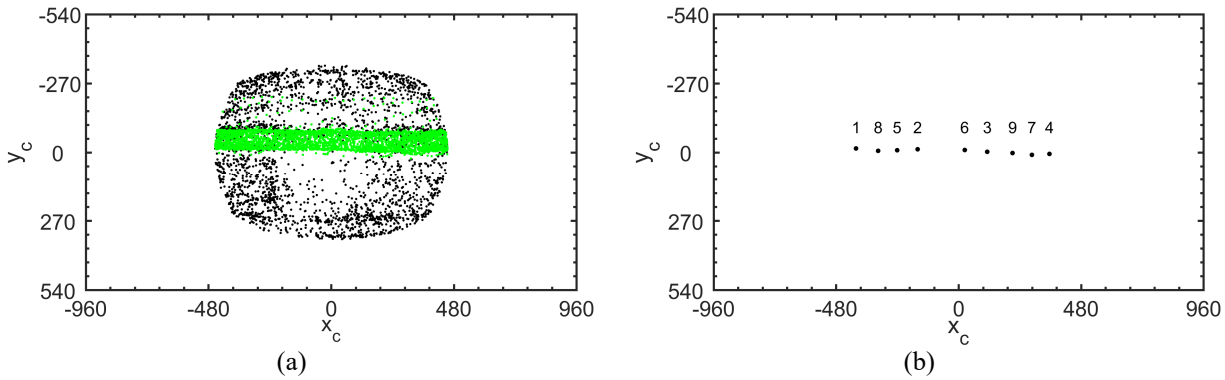

(a) (b)

Figure 9: (a) Image plane with the detected Sun centre coordinates between T+50 s and T+280 s and (b) sequence of nine detected Sun centre coordinates during three revolutions of the spinning sounding rocket. Only the green points are flagged as valid and are used for the 3D orientation estimation

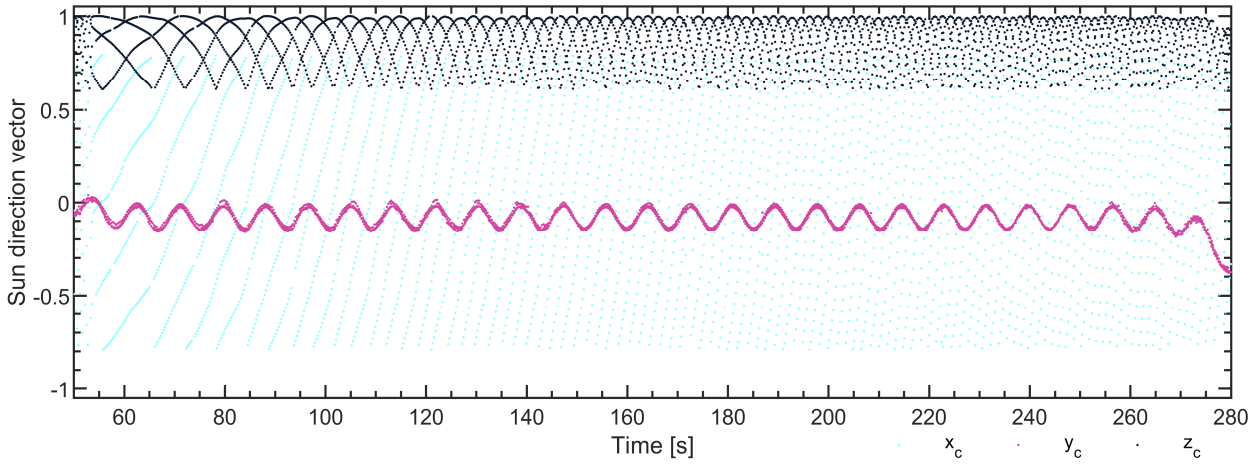

Figure 10: Components of the Sun direction vector $\tilde{\mathbf{e}}_{\mathrm{sun},c}$ in the coasting phase between T+50 s and T+280 s

6. Orientation estimation

6.1 TRIAD method

At the times when the Earth's horizon and the Sun are simultaneously visible on the image, two direction vector observations are simultaneously available and the TRIAD method [4] can readily be used to estimate the three rotational DoF. For the PMWE-2 campaign, the TRIAD method worked well because the Sun was low at about 17 deg elevation at the time of launch on the morning of 1st October. The Earth nadir vector, pointing downwards to the centre of the Earth, and the Sun direction vector, pointing almost horizontally, were nearly orthogonal to each other, resulting in consistent and best possible accuracies of the three rotational DoF estimates.

To use the TRIAD method, the Earth nadir and Sun direction vectors are once required as observed vectors in the vehicle-fixed b-frame, using the transformation matrix $\mathbf{R}_{bc}$ to transform the measured vectors from c- to b-frame,

$$\begin{aligned} \tilde{\mathbf{e}}_{\mathrm{hor},b} &= \mathbf{R}_{bc}\,\tilde{\mathbf{e}}_{\mathrm{hor},c} \\ \tilde{\mathbf{e}}_{\mathrm{sun},b} &= \mathbf{R}_{bc}\,\tilde{\mathbf{e}}_{\mathrm{sun},c} \end{aligned} \tag{5}$$

and once required as expected vectors in the Earth-fixed s-frame

DOI: 10.13009/EUCASS2022-6054

$$\hat{\mathbf{e}}_{\mathrm{hor},s} = -\mathbf{R}_{es}^{\mathrm{T}} \frac{\tilde{\mathbf{x}}_e}{\|\tilde{\mathbf{x}}_e\|} = \begin{pmatrix} 0 \\ 0 \\ 1 \end{pmatrix}$$
$$\hat{\mathbf{e}}_{\mathrm{sun},s} = \mathbf{R}_{es}^{\mathrm{T}} \frac{\mathbf{X}_e - \tilde{\mathbf{x}}_e}{\|\mathbf{X}_e - \tilde{\mathbf{x}}_e\|} \tag{6}$$

where $\mathbf{X}_e$ is the position of the Sun and $\tilde{\mathbf{x}}_e$ is the position of the sounding rocket provided, for example, by the GNSS receiver at the current time t. The transformation matrix $\mathbf{R}_{sb}$ is then calculated from the matrices $\mathbf{A}$ and $\mathbf{B}$ by

$$\mathbf{A} = \left(\hat{\mathbf{e}}_{\mathrm{hor},s} \mid \hat{\mathbf{e}}_{\mathrm{sun},s} \mid \hat{\mathbf{e}}_{\mathrm{hor},s} \times \hat{\mathbf{e}}_{\mathrm{sun},s} \right)$$
$$\mathbf{B} = \left(\tilde{\mathbf{e}}_{\mathrm{hor},b} \mid \tilde{\mathbf{e}}_{\mathrm{sun},b} \mid \tilde{\mathbf{e}}_{\mathrm{hor},b} \times \tilde{\mathbf{e}}_{\mathrm{sun},b} \right) \tag{7}$$
$$\mathbf{R}_{sb} = \mathbf{A} \cdot \mathbf{B}^{-1}$$

The three rotation angles φ_{sb}, ϑ_{sb} and ψ_{sb} can be extracted from the estimated transformation matrix $\mathbf{R}_{sb}$ afterwards and are plotted in Figure 11. Note that the angle ψ_{sb} only covers the range between –155 deg and –50 deg, which corresponds to a range of the y_b-axis w.r.t. North of 115 deg to 220 deg, which is well symmetric to the position of the Sun in the South at an azimuth of about 169 deg.

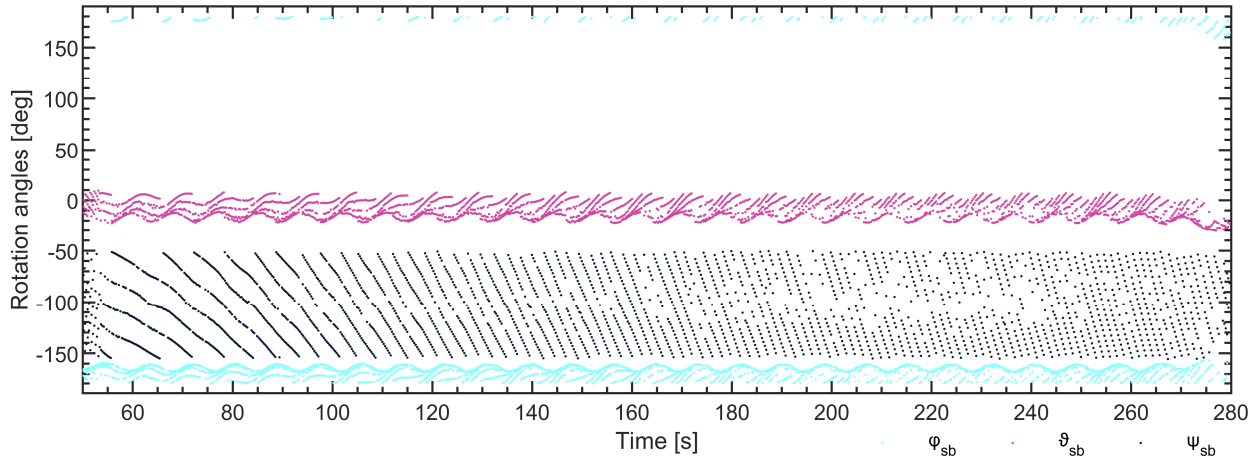

Figure 11: Rotation angles estimated with the TRIAD method when the Earth's horizon and the Sun are simultaneously visible on the image

6.2 Determination of two rotational DoF in the period between simultaneous Earth nadir and Sun direction vector observations

At times when only the Earth's horizon is visible on the image but not the Sun, the TRIAD method cannot be used to estimate the transformation matrix $\mathbf{R}_{sb}$. However, at least two of the three rotational DoF, namely the rotation angles φ_{sb} and ϑ_{sb}, can be determined from the Earth nadir vector observations. Only the third rotational DoF, which is the rotational DoF about the Earth nadir vector itself, cannot be estimated. Due to the advantageous choice of the s-fame as Earth-fixed reference coordinate system, this is just the rotation angle ψ_{sb} around the z_s-axis.

The expected Earth nadir vector transformed to s-frame and to s'-frame takes the simple forms

$$\hat{\mathbf{e}}_{\mathrm{hor},s} = \mathbf{R}_{es}^{\mathrm{T}} \, \hat{\mathbf{e}}_{\mathrm{hor},e} = \begin{pmatrix} 0 \\ 0 \\ 1 \end{pmatrix}, \quad \hat{\mathbf{e}}_{\mathrm{hor},s'} = \begin{pmatrix} 0 \\ 0 \\ 1 \end{pmatrix} \tag{8}$$

By transforming the measured Earth nadir vector $\tilde{\mathbf{e}}_{\mathrm{hor},b}$ into the expected Earth nadir vector $\hat{\mathbf{e}}_{\mathrm{hor},s'}$

DOI: 10.13009/EUCASS2022-6054

$$\begin{pmatrix} 0 \\ 0 \\ 1 \end{pmatrix} = \mathbf{R}_{s'b} \begin{pmatrix} \tilde{e}_{\mathrm{hor},x,b} \\ \tilde{e}_{\mathrm{hor},y,b} \\ \tilde{e}_{\mathrm{hor},z,b} \end{pmatrix} \tag{9}$$

the two rotation angles φ_{sb} and ϑ_{sb}, can be determined. The transformation matrix is

$$\begin{aligned} \mathbf{R}_{s'b} = \mathbf{R}_2\left(\vartheta_{sb}\right)\mathbf{R}_1\left(\varphi_{sb}\right) &= \begin{pmatrix} \cos\vartheta_{sb} & 0 & \sin\vartheta_{sb} \\ 0 & 1 & 0 \\ -\sin\vartheta_{sb} & 0 & \cos\vartheta_{sb} \end{pmatrix} \begin{pmatrix} 1 & 0 & 0 \\ 0 & \cos\varphi_{sb} & -\sin\varphi_{sb} \\ 0 & \sin\varphi_{sb} & \cos\varphi_{sb} \end{pmatrix} \\ &= \begin{pmatrix} \cos\vartheta_{sb} & \sin\varphi_{sb}\sin\vartheta_{sb} & \cos\varphi\sin\vartheta_{sb} \\ 0 & \cos\varphi_{sb} & -\sin\varphi_{sb} \\ -\sin\vartheta_{sb} & \sin\varphi_{sb}\cos\vartheta_{sb} & \cos\varphi_{sb}\cos\vartheta_{sb} \end{pmatrix} \end{aligned} \tag{10}$$

which results in the three equations

$$\begin{aligned} \cos\vartheta_{sb}\ \tilde{e}_{\mathrm{hor},x,b} + \sin\varphi_{sb}\sin\vartheta_{sb}\ \tilde{e}_{\mathrm{hor},y,b} + \cos\varphi_{sb}\sin\vartheta_{sb}\ \tilde{e}_{\mathrm{hor},z,b} &= 0 \\ \cos\varphi_{sb}\ \tilde{e}_{\mathrm{hor},y,b} - \sin\varphi_{sb}\ \tilde{e}_{\mathrm{hor},z,b} &= 0 \\ -\sin\vartheta_{sb}\ \tilde{e}_{\mathrm{hor},x,b} + \sin\varphi_{sb}\cos\vartheta_{sb}\ \tilde{e}_{\mathrm{hor},y,b} + \cos\varphi_{sb}\cos\vartheta_{sb}\ \tilde{e}_{\mathrm{hor},z,b} &= 1 \end{aligned} \tag{11}$$

From the second of the three equations, the angle φ_{sb} can be calculated with

$$\varphi_{sb} = \operatorname{arctan2}\left(\tilde{e}_{\mathrm{hor},y,b}, \tilde{e}_{\mathrm{hor},z,b}\right) = \begin{cases} 2\arctan\dfrac{\sqrt{\tilde{e}_{\mathrm{hor},y,b}^2 + \tilde{e}_{\mathrm{hor},z,b}^2} - \tilde{e}_{\mathrm{hor},z,b}}{\tilde{e}_{\mathrm{hor},y,b}} & , \quad \tilde{e}_{\mathrm{hor},y,b} \neq 0 \\ 0 & , \quad \tilde{e}_{\mathrm{hor},y,b} = 0 \end{cases} \tag{12}$$

With the angle φ_{sb}, the angle ϑ_{sb} is calculated from the first equation

$$\vartheta_{sb} = \begin{cases} \arctan\dfrac{-\tilde{e}_{\mathrm{hor},x,b}}{\sin\varphi_{sb}\ \tilde{e}_{\mathrm{hor},y,b} + \cos\varphi_{sb}\ \tilde{e}_{\mathrm{hor},z,b}} & , \quad \sin\varphi_{sb}\ \tilde{e}_{\mathrm{hor},y,b} + \cos\varphi_{sb}\ \tilde{e}_{\mathrm{hor},z,b} \neq 0 \\ 0 & , \quad \sin\varphi_{sb}\ \tilde{e}_{\mathrm{hor},y,b} + \cos\varphi_{sb}\ \tilde{e}_{\mathrm{hor},z,b} = 0 \end{cases} \tag{13}$$

The third equation is automatically fulfilled. The two rotation angles are illustrated in Figure 12.

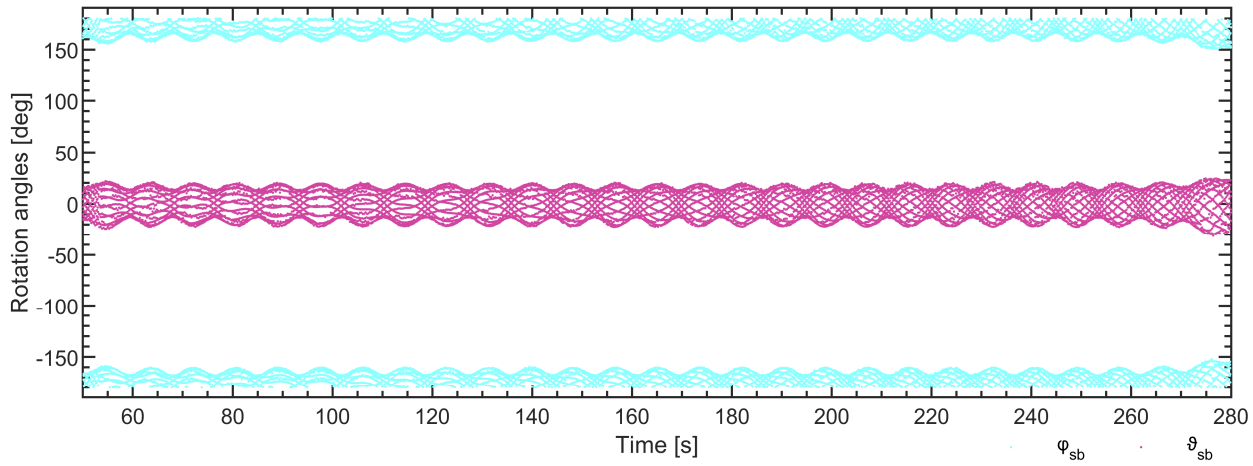

Figure 12: Rotation angles φ_{sb} and ϑ_{sb} during the phases when only the Earth's horizon is visible on the image

DOI: 10.13009/EUCASS2022-6054

6.3 Time interpolation of third rotational DoF about the Earth nadir vector in the period between simultaneous Earth nadir and Sun direction vector observations

In order to obtain all three rotational DoF and thus the 3D orientation of the sounding rocket for all times, i.e. also in the phases where only the Earth's horizon but not the Sun is visible, the rotation angle ψ_{sb} is now interpolated over time. The rotation angles ψ_{sb} calculated with the TRIAD method at the points in time at which both the Earth's horizon and the Sun are visible on the image serve as sample points for the interpolation. The interpolation is done by means of a cubic spline. In Figure 13, the interpolated rotation angle ψ_{sb} is plotted.

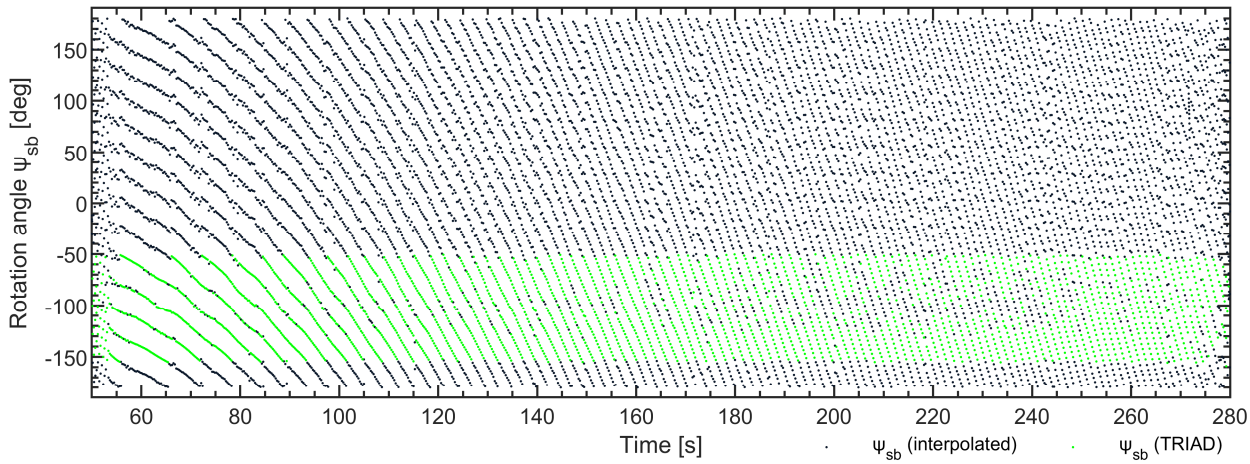

Figure 13: Rotation angle ψ_{sb} interpolated over time. The green points are the sample points for the interpolation

7. Results

As a result, all three rotation angles φ_{sb}, ϑ_{sb} and ψ_{sb} are estimated and the transformation matrix $\mathbf{R}_{sb}$ is fully determined for all times, i.e. for each camera image. The transformation matrix $\mathbf{R}_{eb}$ may easily be obtained by

$$\mathbf{R}_{eb}\left(\varphi_{eb},\vartheta_{eb},\psi_{eb}\right)=\mathbf{R}_{es}\left(\lambda,\theta\right)\cdot\mathbf{R}_{sb}\left(\varphi_{sb},\vartheta_{sb},\psi_{sb}\right) \tag{14}$$

or the transformation matrix $\mathbf{R}_{nb}$ by

$$\mathbf{R}_{nb}\left(\varphi_{nb},\vartheta_{nb},\psi_{nb}\right)=\mathbf{R}_{en}^{\mathrm{T}}\left(\lambda,\phi\right)\cdot\mathbf{R}_{es}\left(\lambda,\theta\right)\cdot\mathbf{R}_{sb}\left(\varphi_{sb},\vartheta_{sb},\psi_{sb}\right) \tag{15}$$

with ϕ being the WGS84 latitude and $\mathbf{R}_{en}$ taking the same form as (3). From $\mathbf{R}_{nb}$, the rotation angles φ_{nb}, ϑ_{nb} and ψ_{nb}, which are commonly used to represent the 3D orientation of a vehicle, can be extracted.

The azimuth and elevation angles of the sounding rocket's longitudinal axis with respect to North and the horizontal plane, respectively, are illustrated in Figure 14. It can be seen that the rocket keeps the orientation of its longitudinal axis stable in the coasting flight phase between T+60 s and T+260 s. On average, the elevation is about 73 deg above the horizontal plane and about –53 deg with respect to North. The oscillations are due to superimposed precession motion with a period of about 8.4 s and nutation motion with a period of about 0.27 s. Figure 15 shows the three rotation angles ψ_{nb} about the z-axis, ϑ_{nb} about the y-axis and φ_{nb} about the x-axis between the n-frame and the b-frame. The 3D orientation of the sounding rocket is exemplarily illustrated in Figure 16 for the time T+120 s. The cyan coloured arrow is the x_b-axis, the magenta coloured arrow is the y_b-axis and the black coloured arrow is the z_b-axis. The grey solid line represents the velocity vector. It can be seen that the Earth nadir vector (blue) and the Sun direction vector (yellow) are almost perpendicular which is an ideal precondition for estimating the 3D orientation from two vector observations.

DOI: 10.13009/EUCASS2022-6054

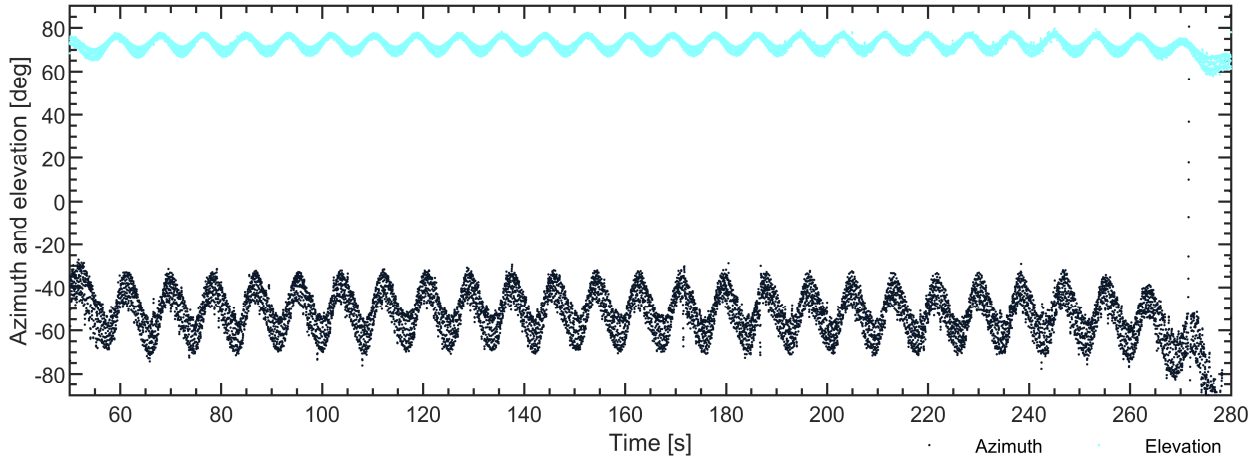

Figure 14: Azimuth and elevation of the sounding rocket's longitudinal axis

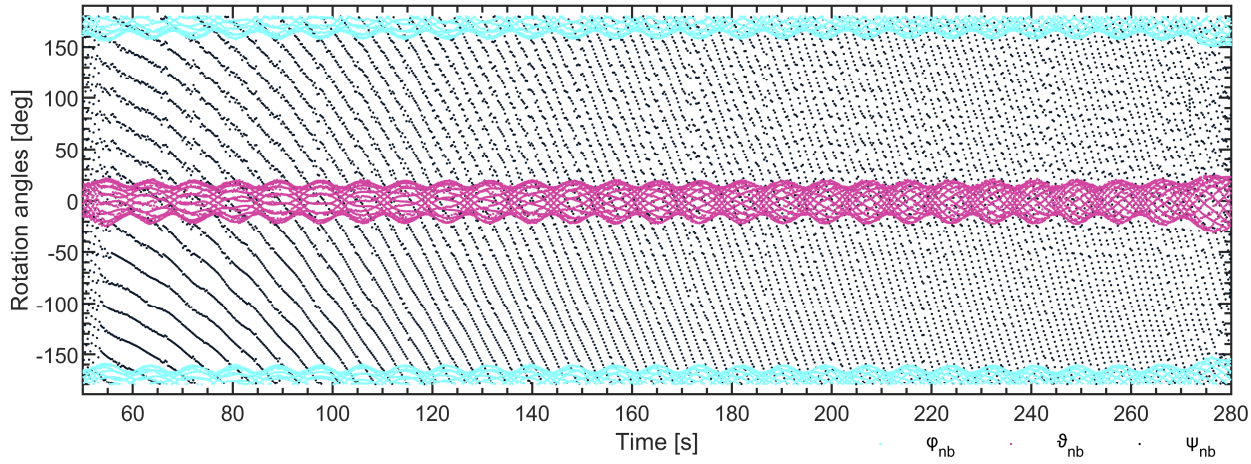

Figure 15: Estimated rotation angles between n-frame and b-frame

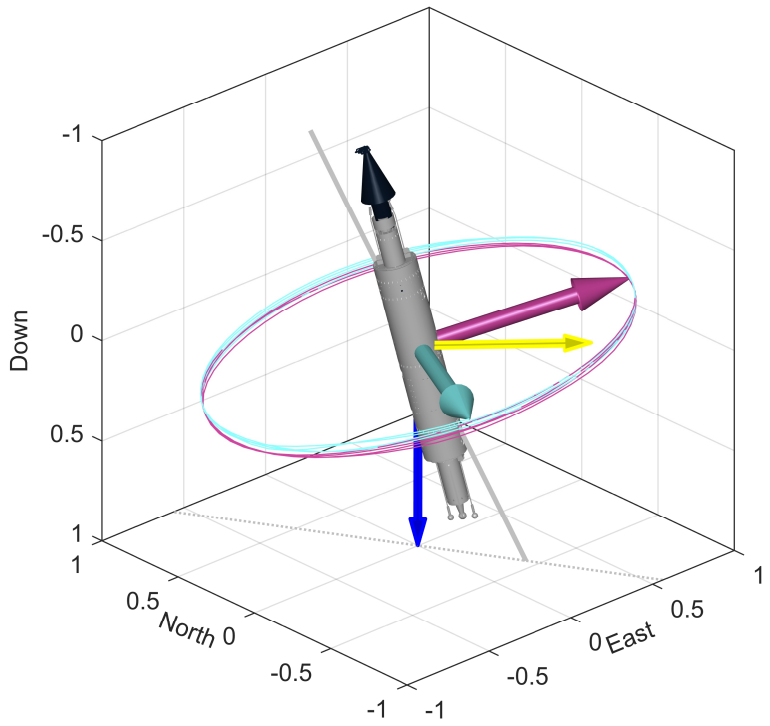

Figure 16: 3D orientation of the sounding rocket exemplarily at T+120 s

DOI: 10.13009/EUCASS2022-6054

8. Conclusion and outlook

The paper presented the estimation of the 3D orientation of the PMWE2F sounding rocket from the Earth nadir and Sun direction vectors extracted from the images of a single side-looking camera. Since the high-grade inertial navigation platform, which was actually intended for providing the orientation, failed immediately after lift-off, at least the 3D orientation estimate from the camera images is available for the post-processing of the scientific measurement data. Although its accuracy is actually lower than that of the inertial navigation platform with about 2 deg (1σ) around all three axes, the 3D orientation estimate still provides additional value to the mission.

Fortunately, due to the late morning launch on an autumn day, the Earth's horizon was well illuminated and the Sun was well visible on the camera images. These good conditions made it possible, at least during the coasting phase, to estimate the 3D orientation solely from the images of the camera. Using optical camera images for orientation estimation requires optimal illumination conditions of the Earth and the visibility of the Sun, which significantly limits the possible lift-off time. Since these constraints often conflict with the scientific requirements of the experiments, they usually cannot be taken into account when choosing the lift-off time, which makes the operational use of camera images for reliable orientation estimation difficult.

But even if not the Earth's horizon and the Sun are both visible on the camera images during a flight, often at least either the Earth's horizon or the Sun are visible, which relaxes the constraints on the lift-off time. While this does not allow the estimation of the full 3D orientation of the sounding rocket, the individual Earth nadir or Sun direction vector measurements can at least be used to aid an integrated navigation system in real-time once they become available. Such an integrated navigation system may consist of a robust strapdown IMU, for example, based on MEMS technology, and a GNSS receiver. The rapidly growing roll angle error about the longitudinal axis, which is unavoidable when using strapdown gyroscopes on spinning sounding rockets, can be observed and reduced by means of the Sun direction vectors. For the Earth's horizon detection, the camera could also be replaced by an infrared camera, which enables the use even during night time, without the need to change the fundamental theory and algorithms for the Earth nadir vector estimation.

The next step toward an operational orientation estimation system is to replace the action camera, which is not designed for the harsh environment of sounding rockets and which had originally been intended for observing the deployment of the recovery chutes, with a more robust camera with a well-defined mount and synchronization with system time. Furthermore, the image processing and orientation estimation algorithms will be prepared for real-time capability.

Acknowledgement

The authors thank the Leibniz Institute of Atmospheric Physics (IAP) and involved partners for their support.

References

[1] Strelnikov, B., Staszak, T., Latteck, R., Renkwitz, T., Strelnikova, I., Lübken, F.-J., Baumgarten, G., Fiedler, J., Chau, J. L., Stude, Rapp, M., Friedrich, M., Gumbel, J., Hedin, J., Belova, E., Hörschgen-Eggers, M., Giono, G., Hörner, I., Löhle, S., Eberhart, M., Fasoulas, S. 2021. Sounding rocket project "PMWE" for investigation of polar mesosphere winter echoes. *Journal of Atmospheric and Solar-Terrestrial Physics*. 218: 105596. doi: 10.1016/j.jastp.2021.105596

[2] Braun, B., Barf, J., Markgraf, M. 2019. Integrated Navigation using MEMS-based Inertial, GPS and Sun Vector Measurements aboard the Spin-Stabilized PMWE-1 Sounding Rocket. *In: Proceedings of the 8th European Conference for Aeronautics and Space Sciences*. doi: 10.13009/EUCASS2019-241

[3] Braun, B., Barf, J. 2022. Image Processing Based Horizon Sensor for Estimating the Orientation of Sounding Rockets, Launch Vehicles and Spacecraft. *CEAS Space Journal.* doi: 10.1007/s12567-022-00461-0

[4] Black, H. D. 1964. A passive system for determining the attitude of a satellite. *AIAA Journal*. 2(7): 1350-1351. doi: 10.2514/3.2555

Supported by:

Federal Ministry
for Economic Affairs
and Climate Action

on the basis of a decision
by the German Bundestag